# CFD Project–4

Rohit Sunil Kanchi[a], Kivanc Ekici[b]

[a]*Student, Department of Mechanical, Aerospace, and Biomedical Engineering, University of Tennessee, Knoxville, TN 37996, USA*
[b]*Professor, Department of Mechanical, Aerospace, and Biomedical Engineering, University of Tennessee, Knoxville, TN 37996, USA*

**Abstract**

In this project, we solve the 2-D Navier-Stokes-Equations (NSE) in vorticity streamfunction formulation in an equispaced computational domain that is mapped to a non uniform curvilinear grid using grid transformation. Details on grid transformation are not in this report. The steady state flow behind cylinder problem is solved and results are compared with those reported in literature. An appreciable match was found. The problem is 2D, steady state using pseudo-time-stepping, second order accurate in space with time integration using the Implicit-Euler method. Finally, we model the time-accurate version of the solver and compare results against literature.

## 1. Governing equations

In this section, we provide details on the governing equation. The non-dimensional governing equations for vorticity-streamfunction in 2D cartesian coordinates are

$$\begin{aligned} \frac{\partial \omega}{\partial \tau} + u\frac{\partial \omega}{\partial x} + v\frac{\partial \omega}{\partial y} &= \frac{1}{Re}\left[\frac{\partial^2 \omega}{\partial x^2} + \frac{\partial^2 \omega}{\partial y^2}\right], \\ \frac{\partial \psi}{\partial \tau} - \frac{\omega}{Re} &= \frac{1}{Re}\left[\frac{\partial^2 \psi}{\partial x^2} + \frac{\partial^2 \psi}{\partial y^2}\right], \end{aligned} \tag{1}$$

where $\omega$ is the vorticity, $\psi$ is the streamfunction, $\tau$ is the pseudo-time, $Re$ is the Reynold's number, $u$ is the horizontal velocity component, $v$ is the vertical velocity component and $x, y$ are the cartesian coordinate variables.

The equations in Eq. (1) work best for uniform grids with equal spacing in Cartesian coordinates. For curviliear grids or non-uniform meshes, the spatial

gradients need transformation. This is achieved through grid transformation techniques. An example of our setup is shown below in Figure 1.

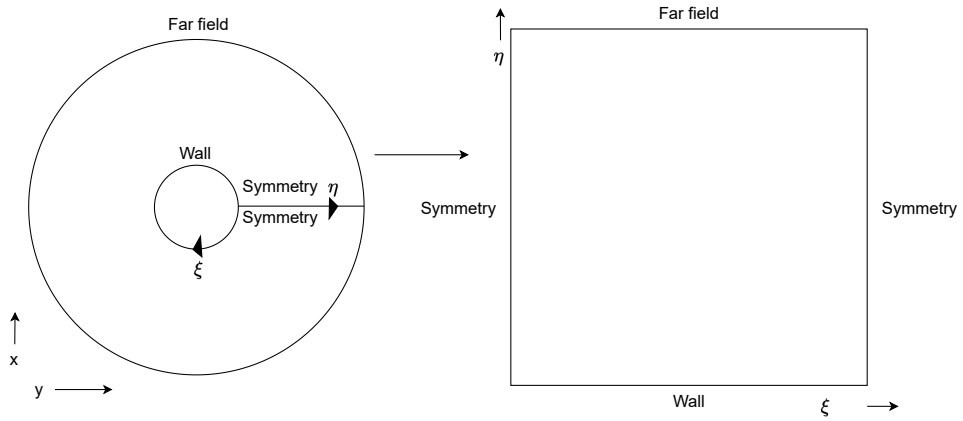


Figure 1: The transformation from physical domain (left) to computational domain(right).

Once the transformation is achieved, the new set of governing equations are

$$\begin{aligned}\frac{\partial \omega}{\partial \tau} + \mathbf{J}\left[\frac{\partial \psi}{\partial \eta}\frac{\partial \omega}{\partial \xi} - \frac{\psi}{\xi}\frac{\omega}{\eta}\right] &= \frac{1}{Re}\left[\boldsymbol{\alpha}\frac{\partial^2 \omega}{\partial \xi^2} + 2\boldsymbol{\gamma}\frac{\partial^2 \omega}{\partial \eta \partial \xi} + \boldsymbol{\beta}\frac{\partial^2 \omega}{\partial \eta^2} + \mathbf{P}\frac{\partial \omega}{\partial \xi} + \mathbf{Q}\frac{\partial \omega}{\partial \eta}\right], \\ -\omega &= \boldsymbol{\alpha}\frac{\partial^2 \psi}{\partial \xi^2} + 2\boldsymbol{\gamma}\frac{\partial^2 \psi}{\partial \eta \partial \xi} + \boldsymbol{\beta}\frac{\partial^2 \psi}{\partial \eta^2} + \mathbf{P}\frac{\partial \psi}{\partial \xi} + \mathbf{Q}\frac{\partial \psi}{\partial \eta},\end{aligned} \tag{2}$$

where $\boldsymbol{\alpha}$, $\boldsymbol{\beta}$, $\boldsymbol{\gamma}$, $\mathbf{P}$, $\mathbf{Q}$ are the transformation metrics, $\mathbf{J}$ is the transformation Jacobian, $\xi$ and $\eta$ are the coordinates of the transformed computational domain, as shown in Figure 1.

The symmetry cut is made at the symmetry plane as shown in Figure 1 in the computational domain and the circle is essentially "unfolded" and edges straightened out to become the domain on the right in Figure 1. Thus, the wall is treated as wall, symmetry is treated as interior points with their respective pointer systems and the far field is treated as a boundary which is literally "far away" from the wall, which is the cylinder in our setup, to make sure that it does not reflect or interfere with our solution. Typically known values of vorticity and streamfunction or gradients of them are specified at these boundaries. In our case of laminar flow, we keep the far field sufficiently far off so the values are prescribed, as will be shown in the next section. The

solution process is exactly the same as in the previous project report of Newton-like iterations till we reach steady state.

## 2. Time accurate simulation methodology

The governing equations for steady state have been described in Section 1. In this section, we will see the equations and what to modify to make the solution time accurate. The governing equations in time accurate sense in cartesian coordinates are given by

$$\begin{aligned} \frac{\partial \omega}{\partial t} + \frac{\partial \omega}{\partial \tau} + u\frac{\partial \omega}{\partial x} + v\frac{\partial \omega}{\partial y} &= \frac{1}{Re}\left[\frac{\partial^2 \omega}{\partial x^2} + \frac{\partial^2 \omega}{\partial y^2}\right], \\ \frac{\partial \psi}{\partial \tau} - \frac{\omega}{Re} &= \frac{1}{Re}\left[\frac{\partial^2 \psi}{\partial x^2} + \frac{\partial^2 \psi}{\partial y^2}\right], \end{aligned} \tag{3}$$

Where $t$ is the non dimensional physical time. This set of equations can be re-written as

$$\begin{aligned} \frac{\partial \omega}{\partial t} + \frac{\partial \omega}{\partial \tau} + \mathbf{V}(\omega, \psi) &= 0, \\ \mathbf{S}(\omega, \psi) &= 0, \end{aligned} \tag{4}$$

where $\mathbf{S}$ and $\mathbf{V}$ are the terms containing the spatial discretizations of vorticity and streamfunction and source terms. Whether post or pre grid-transformation, the system of equations in a Newton-like update is always given as

$$\begin{bmatrix} [\mathbf{A}_{\psi\psi}] & [\mathbf{A}_{\psi\omega}] \\ [\mathbf{A}_{\omega\psi}] & [\mathbf{A}_{\omega\omega}] \end{bmatrix} \begin{bmatrix} [\delta\psi] \\ [\delta\omega] \end{bmatrix} = \begin{bmatrix} \mathbf{b}_\psi \\ \mathbf{b}_\omega \end{bmatrix}. \tag{5}$$

Here, $\mathbf{A}_{\psi\psi}$ is $\partial\mathbf{S}/\partial\psi$, $\mathbf{A}_{\psi\omega}$ is $\partial\mathbf{S}/\partial\omega$, $\mathbf{A}_{\omega\psi}$ is $\partial\mathbf{V}/\partial\psi$ and $\mathbf{A}_{\omega\omega}$ is $\partial\mathbf{V}/\partial\omega$. Since the derivative with repsect to the physical time is only present on the vorticity and rest are all pseudo time derivatives and spatial derivatives, we only need to worry about vorticity. The formulation for streamfunction equation terms $\mathbf{S}$ remains exactly the same.

Discretizing the vorticity equation as shown in Eq. (4) using a second order accurate backward euler scheme for the physical time derivative and

truncating and approximating $\mathbf{V}$ at pseudo time step $i+1$, we have

$$\begin{aligned} &\frac{3\omega_{i+1}^{n+1} - 4\omega^n + \omega^{n-1}}{2\Delta t} + \frac{\omega_{i+1}^{n+1} - \omega_i^{n+1}}{\Delta\tau} \\ &+\frac{\partial \mathbf{V}}{\partial \psi}^{n+1}_{i} \delta\psi + \frac{\partial \mathbf{V}}{\partial \omega}^{n+1}_{i} \delta\omega + \mathbf{V}(\omega_i^{n+1}, \psi_i^{n+1}) = 0, \end{aligned} \tag{6}$$

where $i$ is the pseudo time iteration level and $n$ is the physical time iteration level. Applying some simplifications and algebra, we end up with a simple addition of two terms, one for LHS and one for RHS of Eq. (5) as

$$\begin{bmatrix} \left[\frac{\partial \mathbf{S}}{\partial \psi}^{n+1}_{i}\right] & \left[\frac{\partial \mathbf{S}}{\partial \omega}^{n+1}_{i}\right] \\ \left[\frac{\partial \mathbf{V}}{\partial \psi}^{n+1}_{i}\right] & \left[\frac{\partial \mathbf{V}}{\partial \omega}^{n+1}_{i} + \frac{3}{2\Delta t}\right] \end{bmatrix} \begin{bmatrix} [\delta\psi] \\ [\delta\omega] \end{bmatrix} = \begin{bmatrix} -\mathbf{S}(\omega_i^{n+1}, \psi_i^{n+1}) \\ -\mathbf{V}(\omega_i^{n+1}, \psi_i^{n+1}) - \frac{3\omega_i^{n+1} - 4\omega^n + \omega^{n-1}}{2\Delta t} \end{bmatrix}. \tag{7}$$

Thus, we end up having a main for loop that drives the physical time stepping and an inner while loop that runs the pseudo iterations till convergence. Once the convergence has been achieved for current time step, $\omega^{n-1} = \omega^n$ and $\omega^n = \omega^{n+1}$ where $n+1$ is the current physical time step that just finished converging. This process repeats till the desired number of time-steps have been solved for.

## 3. Boundary condtions

In this section, we derive the boundary conditions for the computational domain.

### *3.1. Symmetry boundaries*

On the left and right boundaries, the exact same equations are solved as are for the interior grid points. The only change is the pointer system. The

pointer system for interior grid points is

$$\begin{aligned} kc &= i + (j-1) \times imax, \\ ke &= k + 1, \\ kw &= k - 1, \\ kn &= k + imax, \\ ks &= k - imax, \\ kne &= kn + imax, \\ knw &= kw - imax, \\ kse &= ks + imax, \\ ksw &= ks - imax, \end{aligned} \tag{8}$$

where $k$ is the pointer, $kc$ is for the current node, $n$ stands for north node, $ne$ stands for north east node and so on. $imax$ is the maximum number of elements along the $\xi$ direction. $jmax$ is the maximum number of elements along the $\eta$ direction. The north-east, north west like pointers are required for computation of cross derivative term $\partial\Phi/\partial\xi\eta$ as shown in Eq. (2). For the symmetry boundaries, th only pointers that change for the left symmetry boundary are

$$\begin{aligned} kw &= kc + imax - 2, \\ knw &= kn + imax - 2, \\ ksw &= ks + imax - 2, \end{aligned} \tag{9}$$

and similarly for the right symmetry boundary as

$$\begin{aligned} ke &= kc - imax + 2, \\ kne &= kn - imax + 2, \\ kse &= ks - imax + 2, \end{aligned} \tag{10}$$

where the rest of the pointers remain exactly the same. This enforces symmetry.

*3.2. Far field*

The far field boundary is basically the top boundary in the computational domain as shown to the right in Figure 1. At this boundary, the $u$-velocity

is non-dimensional value of 1 and $v$-velocity is zero. This means that

$$\begin{aligned} \frac{\partial psi}{\partial y} &= u = 1, \\ \frac{\partial psi}{\partial x} &= v = 0, \end{aligned} \tag{11}$$

which would imply that

$$\begin{aligned} \frac{\mathrm{d}\psi}{\mathrm{d}y} &= 1, \\ \implies \mathrm{d}\psi &= \mathrm{d}y, \end{aligned} \tag{12}$$

where the partial derivative got converted to total, because the dependency reduced to one variable $x$ only. Thus upon integrating and setting the value of $\psi = 0$ at the far field boundary point in line with the cylinder's leading edge, we eliminate the constant of integration and get

$$\psi_k = y_{farfield,k}, \tag{13}$$

where $k$ is the pointer for the node on the far-field boundary. Thus, the value of the stream function at the node on the far-field boundary is simply the $y$-ordinate value of that node. As far as the vorticity is concerned, since we have only horizontal velocity and no vertical velocity at the boundary points on far field, and the fluctuations die out from flow past the cylinder given the free stream and far from body setup, it is safe to assume that the vorticity is zero. Thus, $\omega = 0$ at far field.

### *3.3. Wall*

This is the most tedious of all boundaries. For the wall, we enforce no-slip boundary condition and also specify a tangential rotational velocity $u_{rot}$. To make this work, we employ the following methods.

Before we proceed, it is to be noted that the wall is a continous loop of the circle, which is the cross section of the cylinder in 2D. Thus, we can only physically have one value of stream function at this wall. The stream line from the farfield in line with the leading edge is at zero and that flow will impinge onto the cylinder. Since it was set to zero, we set the value of the stream function at wall to zero as well, else the flow will be unphysical. Thus, $\psi = 0$ all along the wall.

For the vorticity boundary condition, consider the vorticity equation

from Eq. (2). In this equation, the $\partial\psi/\partial xi$ and the higher order derivatives of this reduce to zero, as the stream function is set to zero as aformentioned and this value remains constant along the boundary.

Thus, the equation for vorticity at the wall reduces to

$$-\omega_k = \beta_k \frac{\partial^2 \psi_k}{\partial \eta^2} + Q_k \frac{\partial \psi_k}{\partial \eta}, \tag{14}$$

where $k$ is the node pointer at wall node. We have previously derived the second order accurate one-sided finite difference for $\partial^2\psi_k/\partial\eta^2$ as

$$\frac{\partial^2 \psi_k}{\partial \eta^2} = \frac{-7\psi_k + 8\psi_{kn} - \psi_{knn}}{2(\Delta\eta)^2} - \frac{3}{\Delta\eta}\frac{\partial \psi}{\partial \eta}, \tag{15}$$

where $k$ is the pointer at wall, $kn$ and $knn$ are the points into the domain at north and north of the point at north.

In radial coordinates, $u_\theta = -\partial\psi/\partial r$ and $u_r = (1/r)(\partial\psi/\partial\theta)$. During cylinder rotation, it only rotates but does not stretch. Thus, $u_r = 0$. Applying chain rule, we have

$$\frac{\partial \psi}{\partial r} = \frac{\partial \psi}{\partial \xi}\frac{\partial \xi}{\partial x}\frac{\partial x}{\partial r} + \frac{\partial \psi}{\partial \eta}\frac{\partial \eta}{\partial x}\frac{\partial x}{\partial r} + \frac{\partial \psi}{\partial \xi}\frac{\partial \xi}{\partial y}\frac{\partial y}{\partial r} + \frac{\partial \psi}{\partial \eta}\frac{\partial \eta}{\partial y}\frac{\partial y}{\partial r}, \tag{16}$$

where the derivative $\partial\psi/\partial\xi$ cancels out due to no variation along that direction in at the wall as aformentioned.

Thus, given that $x = rcos(\theta)$ and $y = rsin(\theta)$ we have by plugging these values into the derivatives above

$$\begin{aligned} \frac{\partial \psi_k}{\partial r} &= \frac{\partial \psi_k}{\partial \eta}\Big[\eta_x cos(\theta) + \eta_y sin(\theta)\Big]_k, \\ \implies -u_\theta &= \frac{\partial \psi_k}{\partial \eta}\Big[\eta_x cos(\theta) + \eta_y sin(\theta)\Big]_k, \\ \implies \frac{\partial \psi_k}{\partial \eta} &= \frac{-u_\theta}{\Big[\eta_x cos(\theta) + \eta_y sin(\theta)\Big]_k}, \end{aligned} \tag{17}$$

where $\eta_x = \partial\eta/\partial x$ and $\eta_y = \partial\eta/\partial y$ and these are calculated during the computation of the metrics in Eq. (2).

Thus, plugging the values from Eqs. (15) and (17) into Eq. (14), we have

$$-\omega_k = \beta_k \left[ \frac{-7\psi_k + 8\psi_{kn} - \psi_{knn}}{2(\Delta\eta)^2} \right] + \left[ Q_k - 3\frac{\beta_k}{\Delta\eta} \right] \left[ \frac{-u_\theta}{\eta_x cos(\theta) + \eta_y sin(\theta)} \right]_k \tag{18}$$

## 4. Results and discussion

The mesh for the physical domain is shown below in Figure 2.

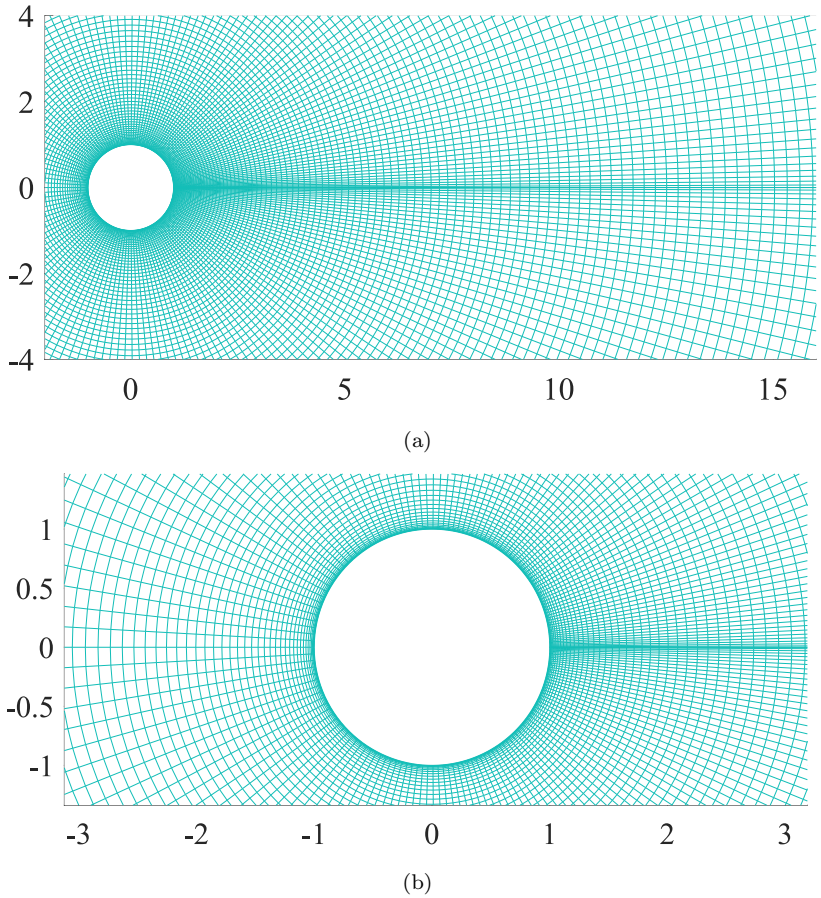


Figure 2: The physical domain pre conversion to the computational domain.

The computational domain is simply the rectangular 2D cartesian equispaced grid as seen before.

The flow behind cylinder for steady state was solved using a Newton-like iterative solver with pseudo time-stepping. As the first case, we solved for Reynold's number $Re$ of 40 and 100. The results for streamlines are shown in Figure 3.

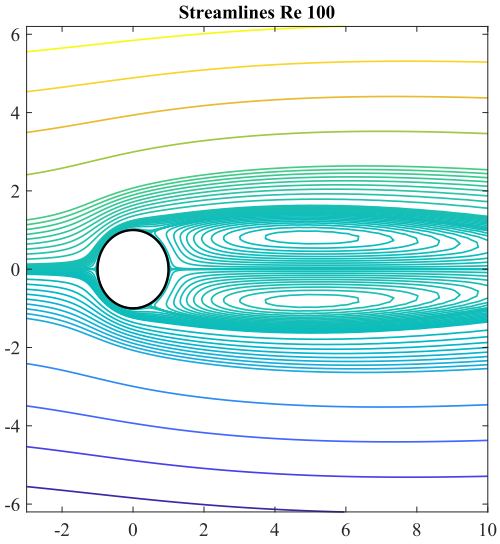


(a) Re = 100

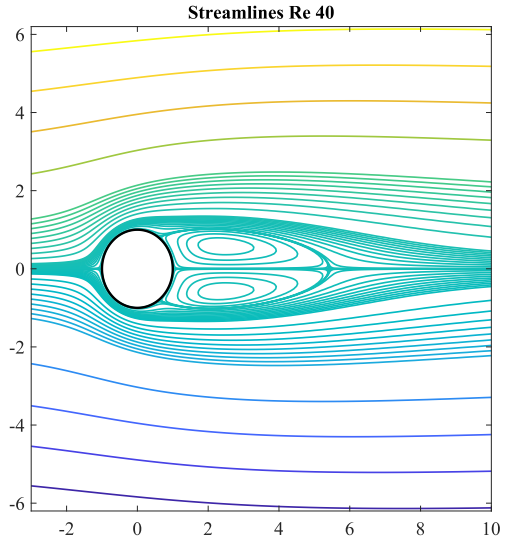


(b) Re = 40

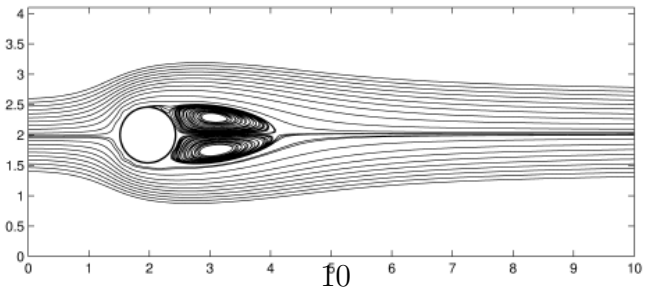


(c) Re = 40 from Xiao et al. [1]

Figure 3: Streamline plots at different Reynolds numbers: (a) Re = 100, (b) Re = 40, and (c) Re = 40 reported from literature by Xiao et al. [1].

The vorticity for the Reynold's numbers 40 and 100 are shown below in

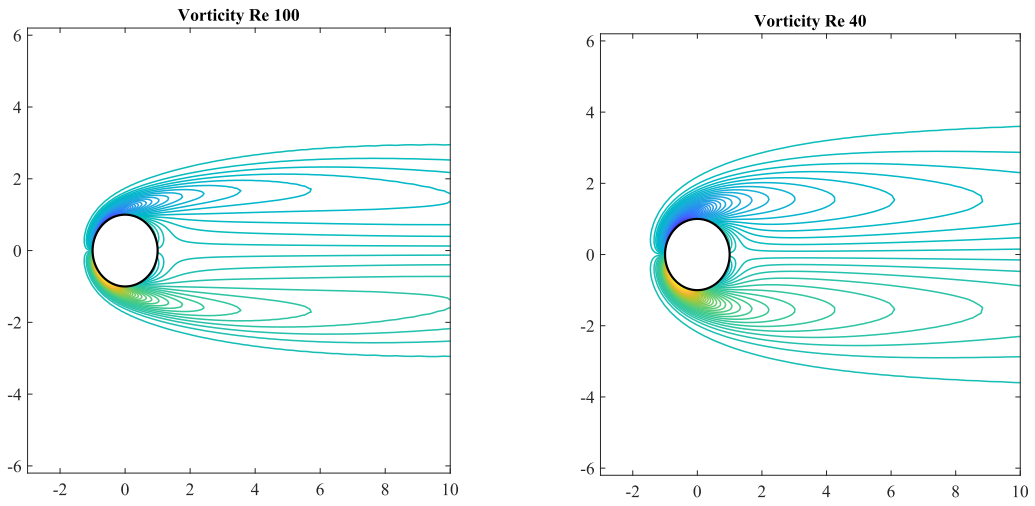


(a) Re = 100 (b) Re = 40

Figure 4: Vorticity contour lines at different Reynolds numbers: (a) Re = 100 and (b) Re = 40.

Six more simulations were run, with three cases for two Reynold's number of 5 and 20. For each Reynold's number of 5 and 20, the first subcase was with no rotation, second was with -0.2 rotational velocity and third with -0.5 rotational velocity. Results from these computations were compared against Ingham's results [2].

The streamlines from the current computations are comapred against those of Ingham's [2] qualitatively below in Figure 5

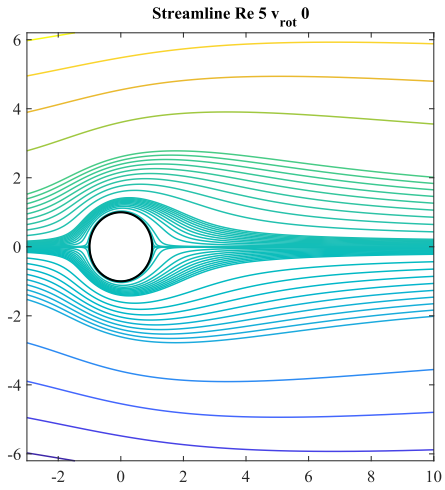


(a)

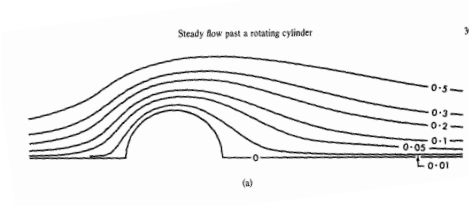


(b)

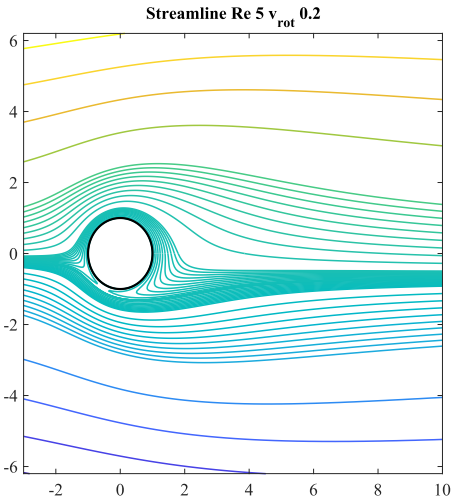


(c)

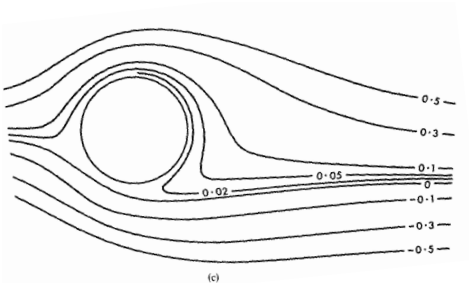


(d)

Figure 5: Streamline comparisons with data from Ingham [2]. (a) and (b) are paired, and (c) and (d) are paired in the comparisons.

The surface vorticity values were plotted against the angles of their locations on the surface of the cylinder. The results are compared against Ingham's [2] below in Figure 6 for Re=5 and in Figure 7 for Re=20.

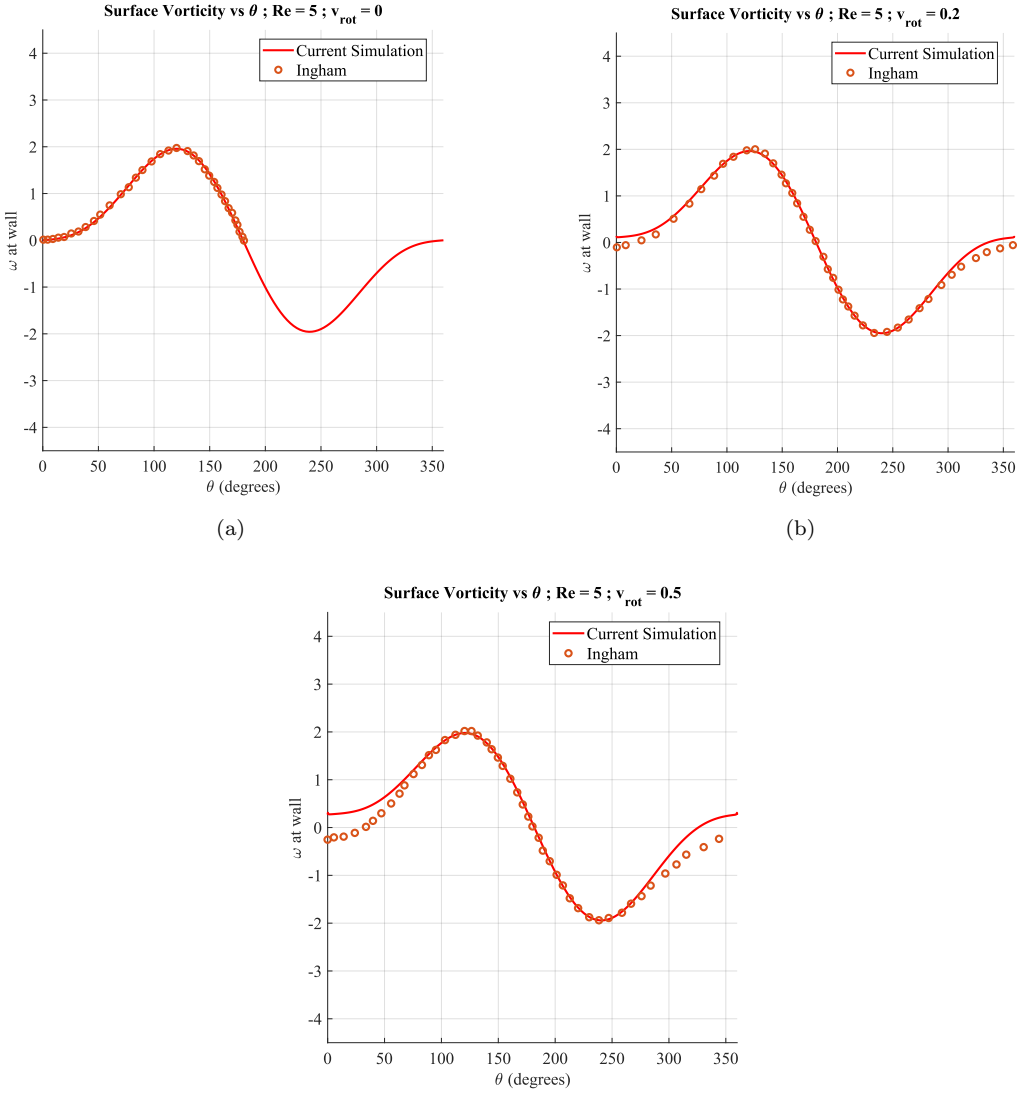


(a) (b)

(c)

Figure 6: Comparison of the surface vorticity values plotted as a function of $\theta$ for Re $= 5$ against those reported by Ingham [2].

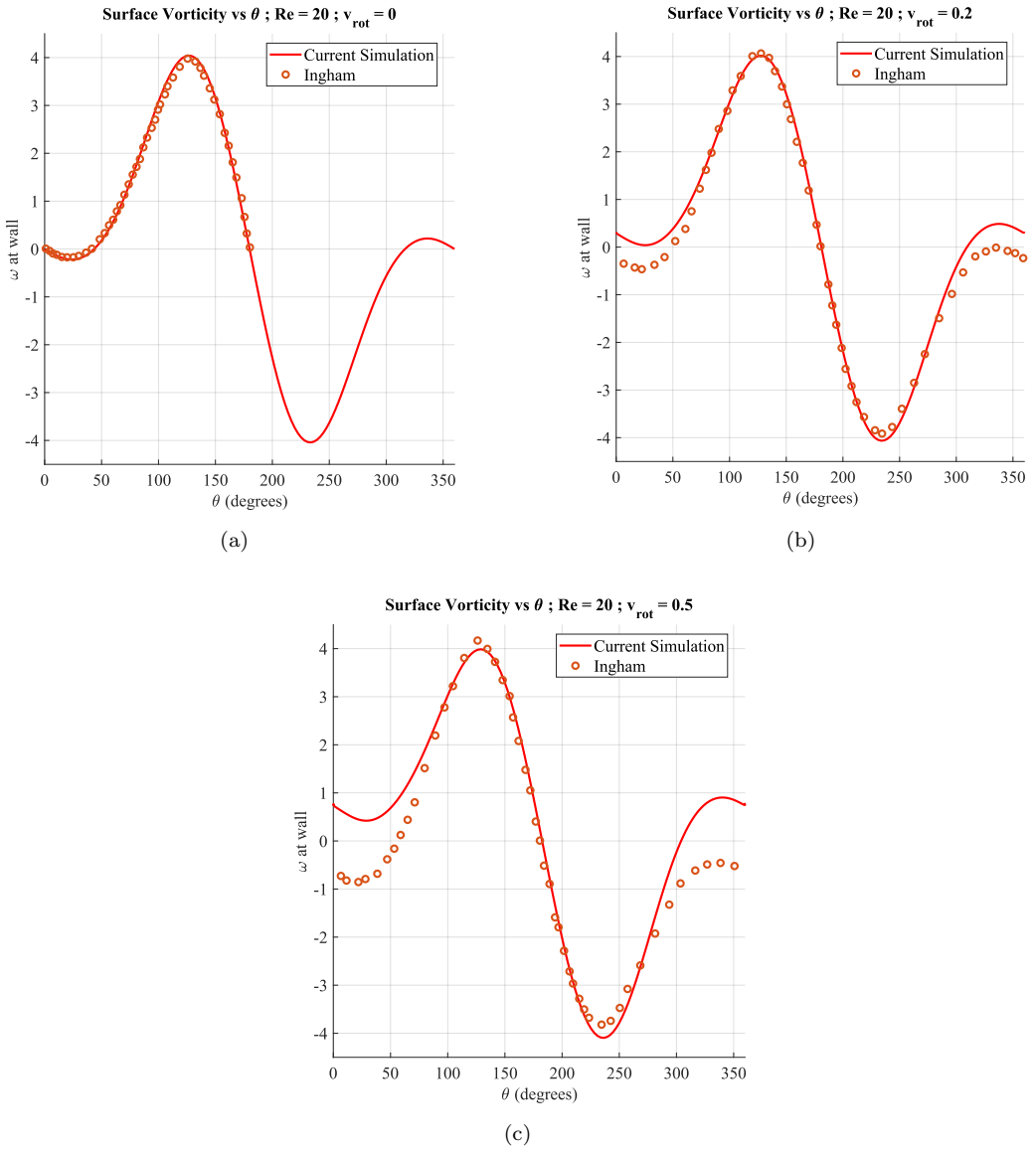


Figure 7: Comparison of the surface vorticity values plotted as a function of $\theta$ for Re = 20 against those reported by Ingham [2].

It is observed that Ingham's mesh [2] was not clustered near the surface and that their mesh was relatively coarse. Further, the solution methods are different which is why in regions of higher strain rate or vorticity, higher Reynold's numbers and higher values of rotational speeds we see that the

solutions are close but do not match with Ingham's results. Nevertheless, an appreciable match was obtained with the current computational methodology employed.

## 5. Time accurate results

In this section, we show the results for the unsteady simulations at Reynold's numbers of 40 and 100. It is expected that there is no vortex shedding at Re=40 and there is vortex shedding at Re=100. In the simulations performed, it was observed that the vortex shedding did not start for long even at Reynolds number of 100. This is because we need to wait for numerical errors to kick in to push the system into limit cycle. To expedite the onset of vortex shedding, the cylinder was rotated at a rotational velocity (non-dimensional again) of 0.5 for two seconds and then stopped. Each simulation was then run for the respective Reynold's numbers for a physical nondimensional time value of 50.

Another point is that the solution scheme is very stable at very high time steps as well, although accuracy is questionable. Nevertheless, a time step of 0.2 was used. A time step of 0.02 was advised in report but this was very time consuming to wait till 50 non-dimensional time. Both results were compared and negligible differences were found and therefore it was decided to proceed with rest of simulations at 0.2 step size.

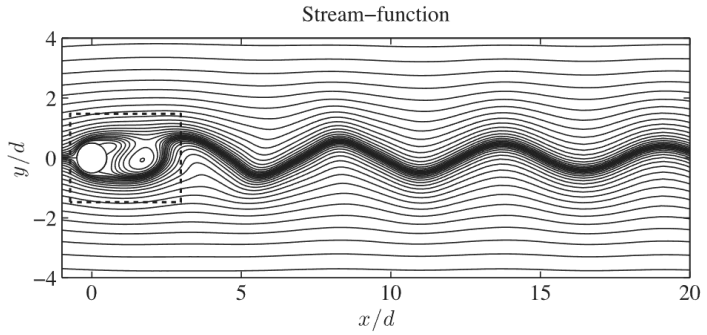


(a)

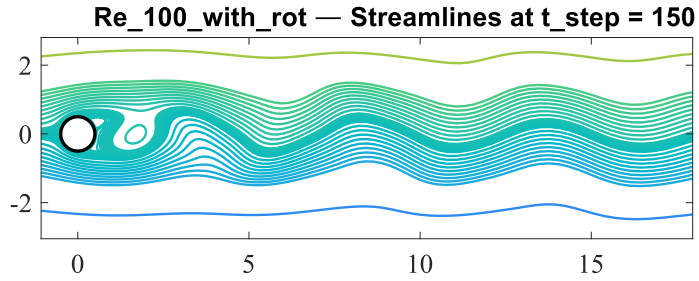


(b)

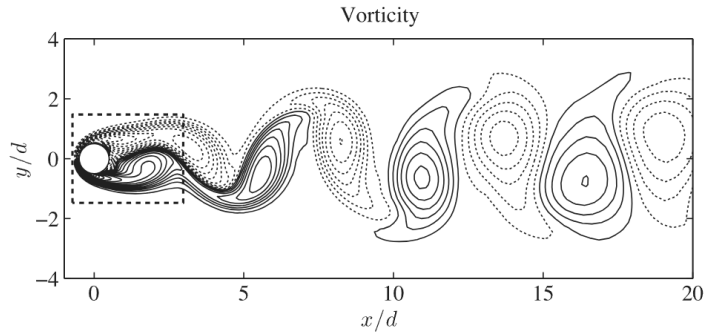


(c)

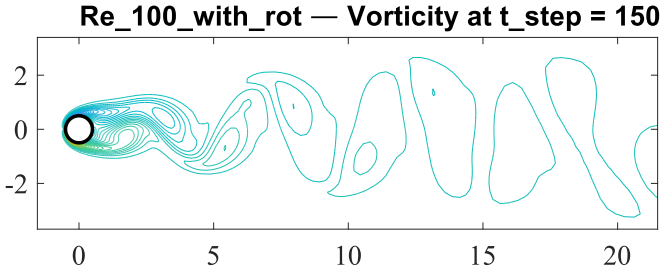


(d)

Figure 8: Comparison of vorticity and streamline contours between current study and Garman and Daniel [3]

Results were plotted for the vorticity contour lines and streamfunction contour lines as shown in Figure 8. Another pair of plots was made for Reynold's number of 100 for the vorticity value probed at a distance of 2 from the cylinder surface along the center horizontal line of the domain at x=0. This was plotted against time as shown in Figure 9. Results are compared against those of Garman and Daniel [3] in both Figures 8 and 9. The frequency of oscillations seems to match that of Garman and Daniel [3] (About 0.16).

Another observation is that if no rotation is given, the contours of Reynolds number of 100 and 40 resemble that of Figure 4. For Reynold's number of 100, the simulation was probably not run long enough for numerical oscillations to kick in and push the system into vortex shedding. As aformentioned, the process of moving from no limit cycle to limit cycle oscillations was expedited by rotating the cylinder initially.

As expected, for Reynold's number of 100, the shedding started and reached saturation. For Re 40, there were initial vortices and therefore the initial transients as can be seen in Figure 9. These transients do oscillate but die out because at Re 40 the cylinder does not shed any vortices being in the laminar regime a few Re numbers before the onset which happens around 47-50.

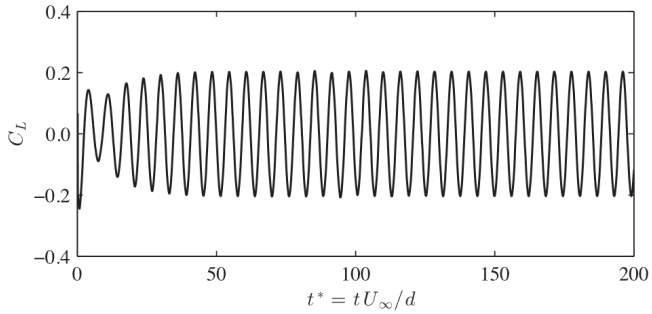


(a)

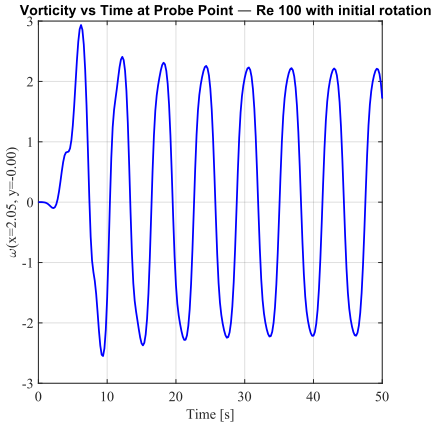


(b)

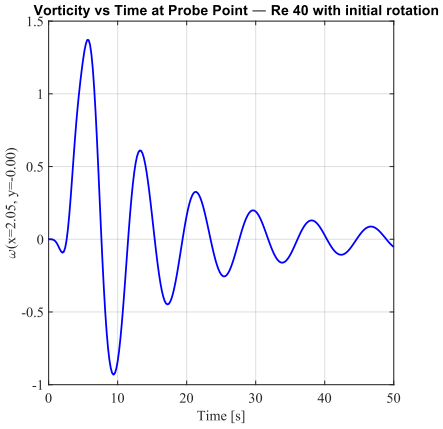


(c)

Figure 9: Comparison of oscillations and frequency between current study and Garman and Daniel's [3]

## 6. Conclusion

In this project, we undertook the solution to the Navier-Stokes equations in 2D for an incompressible viscous fluid and solved it with the help of vorticity-stream function formulation to remove the issue of pressure-velocity coupling, essentially reducing the system of equations to two equations, the vorticity-streamfunction equation and the vorticity transport equation.

The equations were discretized first order accurate in pseudo time and second order finite differences in space at interior and boundaries as well. All the terms were discretized at time level $n+1$. This led to a fully-implicit solution. Block matrix form was taken to solve the vorticity and stream equations together in one shot in each iteration, leading to a fully-coupled solution.

In the previous project, we solved the lid-driven cavity problem on a uniform mesh. The robustness of the Newton iteration approach was highlighted. In this project, we employed the very same solution methodology but the equations were slightly modified as the solution was on the transformed computational domain from the exisiting physical domain using grid transformation technique.

The problem of flow behind cylinder was solved. The Jacobian along with the metrics of transformation were used with the vorticity stream function formulation and solved in a fully coupled fully implicit Newton-like update method in pseudo time. Results converged in about 6 iterations for all the cases. The results from computations were compared against those in literature and appreciable matches were observed.

In the time accurate simulations, an inner loop of pseudo time iterations were performed till convergence for each time step, wherein the time stepping happened in the outer loop. The time accurate simulations were second order accurate in time backward euler and used two time steps in history with current time level in simulation. The solver is very stable at high time step sizes which aided in faster analysis and convergence. The Newton-like iteration procedure with inifite time step size in pseudo time if ran correctly gaurantees convergence in the inner iterations. Similar to the steady state results, matches were obtained when the results from time accurate simulations were compared against the literature data.

## References


[1] M. Xiao, M. Novy, J. Myatt, S. Banda, A rotary control of the circular cylinder wake: An analytic approach, in: 1st Flow Control Conference, American Institute of Aeronautics and Astronautics, 2002. doi:10.2514/6.2002-3075.

[2] D. Ingham, Steady flow past a rotating cylinder, Computers amp; Fluids 11 (1983) 351–366. doi:10.1016/0045-7930(83)90020-8.

[3] D. J. Garmann, Compact finite-differencing and filtering procedure applied to the incompressible navier-stokes equations, AIAA Journal 51 (2013) 2241–2251. doi:10.2514/1.j052264.